

# REDDENING BEHAVIORS OF GALAXIES IN THE SDSS PHOTOMETRIC SYSTEM

SUNGSOO S. KIM<sup>1</sup> AND MYUNG GYOON LEE<sup>2</sup>

*Published in PASP, 119, 1449 (Dec. 2007)*

## ABSTRACT

We analyze the behaviors of reddening vectors in the SDSS photometric system for galaxies of different morphologies, ages, and redshifts. As seen in other photometric systems, the dependence of reddening on the spectral energy distribution (SED) and the nonlinearity of reddening are likewise non-negligible for the SDSS system if extinction is significant ( $\gtrsim 1$  mag). These behaviors are most significant for the  $g$  filter, which has the largest bandwidth-to-central wavelength ratio among SDSS filters. The SDSS colors involving adjacent filters show greater SED-dependence and nonlinearity. A procedure for calculating the correct amount of extinction from an observed color excess is provided. The relative extinctions between (i.e., the extinction law for) SDSS filters given by Schlegel et al., which were calculated with an older version of filter response functions, would underestimate the amount of extinction in most cases by  $\sim 5$  to 10 % (maximum  $\sim 20$  %). We recommend  $A/A_{5500\text{\AA}}$  values of 1.574, 1.191, 0.876, 0.671, & 0.486 for the  $u$ ,  $g$ ,  $r$ ,  $i$ , &  $z$  filters, respectively, as a representative extinction law for the SDSS galaxies with a small extinction (i.e., for cases where the nonlinearity and SED-dependence of the reddening is not important). The dependence of reddening on redshift at low extinction is the largest for colors involving the  $g$  filter as well, which is due to the Balmer break.

*Subject headings:* Hertzsprung-Russell diagram — techniques: photometric — dust, extinction

## 1. INTRODUCTION

The Sloan Digital Sky Survey (SDSS; Stoughton et al. 2002) completed its first phase of operations in June 2005, and has entered a second phase, SDSS-II, which will continue until June 2008. One of the three surveys being carried out by SDSS-II is the Sloan Extension for Galactic Understanding and Exploration (SEGUE), which is currently mapping the structure of the Milky Way. SEGUE will produce 3,500 square degrees of new images, some on a regular grid extending through the Galactic plane and some sampling structures like the Sagittarius dwarf tidal stream. With the information from higher to lower Galactic latitudes sampled on a uniform longitudinal grid, SEGUE will significantly improve our understanding of the thick and thin disks of the Milky Way, as well as of the external galaxies in the zone of avoidance.

The analyses of photometric data from the lower Galactic latitudes, however, will require careful step of removing the effects of the Galactic interstellar extinction. One of the most common ways of estimating the amount of interstellar extinction from photometric data involves a color-magnitude (CM) or color-color (CC) diagram: one measures the amount of color excess and converts it to an extinction value by using a certain extinction law. This procedure seems simple, but care must be taken when the extinction is significant, because the amount of extinction in magnitudes of a certain photometric band depends on the detailed spectral energy distribution (SED) of the object and is moreover not simply proportional to the amount of interstellar dust. The former effect makes the slope of the reddening vector in the

CM or CC diagrams dependent on the type of the object, while the latter makes the reddening vector nonlinear. These effects arise because the transmission functions of the photometric filters have non-negligible bandwidths (i.e. they are not Dirac delta functions), and they hence become more important for wide-band filters.

The first thorough study on the SED dependence and nonlinearity of interstellar extinction was performed by Grebel & Roberts (1995; see the references therein for earlier works on these issues). Using the Kurucz models of synthetic stellar spectra, they derived color-dependent interstellar extinction relations for Johnson-Cousins  $UBVRI$  and Washington  $CMT_1T_2$  photometric systems. They found that the reddenings of main-sequence stars and evolved stars are quite different and also can be nonlinear as functions of color.

While Grebel & Roberts (1995) studied the reddening behaviors of individual stars in the optical bands, Kim et al. (2005) and Kim, Figer, & Lee (2006) investigated the collective behaviors of the reddening for various isochrones in the near-infrared CM diagrams. They found that the reddened isochrones of different ages and metallicities behave as if they follow different extinction laws, and that the reddening vectors of some filter pairs in the CM diagrams (particularly those in the *Hubble Space Telescope* NICMOS) are considerably nonlinear. They provided a so-called “effective extinction slope” for each filter pair and isochrone model as well as the coefficients of the third-order polynomials that best fit the reddening vectors in the NICMOS CM diagrams for various isochrones.

There have been some theoretical studies on the extinction properties of the SDSS photometric system. Schlegel, Finkbeiner, & Davis (1998) and Stoughton et al. (2002), among others, have calculated the extinction ratios  $A_i/A_V$  of five SDSS bands ( $u$ ,  $g$ ,  $r$ ,  $i$ , and  $z$ ) relative to the  $V$  band for a normal elliptical galaxy

<sup>1</sup> Dept. of Astronomy & Space Science, Kyung Hee University, Yongin-shi, Kyungki-do 449-701, Korea; sungsoo.kim@khu.ac.kr

<sup>2</sup> Astronomy Program, Dept. of Physics & Astronomy, Seoul National University, Seoul 151-742, Korea; mglee@astrog.snu.ac.kr

SED. Fiorucci & Munari (2003) provided the minimum and maximum values of  $A_i/A_V$  for several different stars. The dependence of extinction on stellar parameters and the nonlinearity of extinction for SDSS bands were studied by Girardi et al. (2004; GGOC hereafter). Although their main goal was to provide the theoretical isochrones in the SDSS system, they also gave  $A_i/A_V$  values for stars with a few different values of effective temperature  $T_{eff}$ , surface gravity  $\log g$ , and metallicity  $[M/H]$  as well. They calculated  $A_i/A_V$  values for different  $A_V$  values of up to 3 mag as well, but only for one set of stellar parameters. The study by GGOC clearly shows that SED dependence and nonlinearity of extinction are non-negligible for SDSS bands as well.

In the present paper, we extend the study by GGOC and analyze the behavior of reddening in the SDSS photometric system for SEDs of several representative galaxies. We show that the nonlinearity and the SED-dependence of the reddening is not negligible for the SDSS filters. Our results are to be used for correctly estimating the amount of extinction. Due to the SED-dependence of the reddening, one needs to know the approximate morphology, age, and redshift of the galaxy before estimating the extinction. For cases where the spectrum or visual classification of morphology is not available, we discuss how one could estimate such information from the photometry.

This paper is composed as follows. We describe our models in § 2, present and discuss our calculations in § 3, and summarize our findings in § 4.

## 2. MODELS

### 2.1. Magnitudes

Following Fukugita et al. (1996) and GGOC, we adopt an AB magnitude system (Oke & Gunn 1983), which has a flat reference spectrum of flux  $f_\nu^0 = f_\lambda^0 \lambda^2 / c = 3.631 \times 10^{-20} \text{ erg s}^{-1} \text{ cm}^{-2} \text{ Hz}^{-1}$  and a reference magnitude  $m_{S_\lambda}^0 = 0$  for all filters. The apparent magnitude  $m_{S_\lambda}$ , as measured using a filter with transmission function  $S_\lambda$ , is given by

$$m_{S_\lambda} = -2.5 \log \left( \frac{\int \lambda f_\lambda S_\lambda d\lambda}{\int \lambda f_\nu^0 S_\lambda d\lambda} \right) + m_{S_\lambda}^0, \quad (1)$$

where the flux of a star measured at the top of the Earth atmosphere,  $f_\lambda$ , is related to the flux at the stellar photosphere,  $F_\lambda$ , by

$$f_\lambda = 10^{-0.4A_\lambda} (R/d)^2 F_\lambda. \quad (2)$$

Here  $A_\lambda$  is the extinction in magnitudes,  $R$  the stellar radius, and  $d$  the distance to the star.

We use the SDSS filter response functions for airmass  $X = 1.3$  available from the SDSS Data Release 5 Web pages.<sup>3</sup> The central wavelength

$$\lambda_c = \exp \frac{\int d(\ln \nu) S_\nu \ln \lambda}{\int d(\ln \nu) S_\nu} \quad (3)$$

(defined by Schneider, Gunn, & Hoessel 1983 as the effective wavelength) and the bandwidth

$$\Delta\lambda = \frac{\int d\lambda S_\lambda}{\max S_\nu} \quad (4)$$

<sup>3</sup> <http://www.sdss.org/dr5/instruments/imager/filters/index.html>.

TABLE 1  
SDSS FILTER PROPERTIES

Filter	<i>u</i>	<i>g</i>	<i>r</i>	<i>i</i>	<i>z</i>
$\lambda_c$ (Å)	3588	4797	6232	7549	9039
$\Delta\lambda$ (Å)	558	1158	1111	1041	1125
$\Delta\lambda/\lambda_c$	0.156	0.241	0.178	0.138	0.124

NOTE. —  $\lambda_c$  and  $\Delta\lambda$  are the central wavelength (eq. 3) and the bandwidth (eq. 4) of the filter, respectively.

of SDSS filters are presented in Table 1. When convolving the SED of isochrones and galaxies with the transmission curve, we adopt the photon integration (eq. 1) instead of the energy integration (eq. 1 without  $\lambda$  in both integrands) as data from the charge-coupled devices would be better represented by the former.

### 2.2. Galaxies

We adopt the stellar population synthesis model by Bruzual & Charlot (2003) for the SEDs of simple stellar populations (SSPs; or instantaneous-burst models) computed using the initial mass function (IMF) given by Chabrier (2003) with lower and upper mass cutoffs of 0.1 and 100  $M_\odot$ , respectively. Then these SSPs are combined to form the SEDs of four different galaxy morphologies, E, Sa, Sb, & Im, following the recipes by Buzzoni (2005). Buzzoni (2005) implemented three  $[\text{Fe}/\text{H}]$  values to build up his galaxy models but those values do not coincide with those used in the SSP models given by Bruzual & Charlot (2003). So, we interpolate the SSP SEDs for the  $[\text{Fe}/\text{H}]$  values used by the Buzzoni models. Figure 1 shows the SEDs for 3 and 10 Gyr template galaxies of four different morphologies constructed in this way.<sup>4</sup>

### 2.3. The Extinction Law

We adopt the extinction law by Cardelli, Clayton, & Mathis (1989) for a typical Galactic total-to-selective ratio of  $R_V \equiv A_V/(A_B - A_V) = 3.1$ . They provide fitting formulae to calculate the amount of interstellar extinction at wavelength  $\lambda$  relative to the one at the  $V$  filter ( $A_\lambda/A_V$ ). But as  $A_V$  also exhibits the SED dependence and nonlinearity, we regard their extinction law as the extinction relative to the one at  $\lambda = 5500 \text{ Å}$  ( $A_\lambda/A_{5500}$ ), which is the pivot wavelength of their extinction formulae. We find that our  $A_\lambda/A_{5500}$  values for select synthetic stellar spectra agree with those of GGOC within 1 % (it appears that the  $A_\lambda/A_V$  values of GGOC is defined in the same way as our  $A_\lambda/A_{5500}$ ).

## 3. REDDENING BEHAVIORS

Now we analyze the reddening behaviors of various galaxy models for  $A_\lambda$  values of up to 5 mag in each SDSS band. We calculate how the magnitudes of our galaxy models change as we increase  $A_{5500}$  and obtain the actual extinction values,  $A^{act}$ , for each SDSS filter. Then the differences and ratios between these  $A^{act}$  values for each galaxy model determine the reddening curves in the CM and CC diagrams (we herein use the term “reddening curve” instead of “reddening vector” to emphasize

<sup>4</sup> An electronic version of our galaxy SEDs is available from the authors upon request.

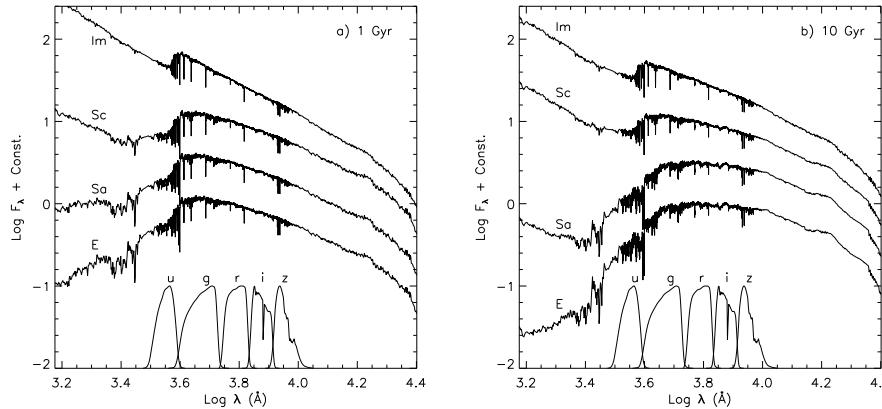

 FIG. 1.— Spectra of our  $z = 0$  galaxy models for four different morphologies at 1 Gyr (a) and 10 Gyr (b).

 TABLE 2  
RELATIVE EXTINCTION FOR SDSS FILTERS

	<i>u</i>	<i>g</i>	<i>r</i>	<i>i</i>	<i>z</i>
Our Reference <sup>a</sup>	1.574	1.191	0.876	0.671	0.486
Schlegel et al. <sup>b</sup>	1.579	1.161	0.843	0.639	0.453

<sup>a</sup>  $A_i/A_{5500}$  values for the SED of a 10 Gyr, elliptical galaxy at redshift  $z = 0$  when  $A_{5500} = 0.1$ .

<sup>b</sup>  $A_i/A_V$  values calculated by Schlegel et al. (1998) for a normal elliptical galaxy SED.

the fact that the actual reddening is not linear in the CM and CC diagrams; we use the term reddening vector only for the “reference reddening vector” described below, which we mean to be linear).

### 3.1. Reddening Estimation from Color Excess

For an object whose intrinsic color can be estimated, the amount of extinction is estimated by transforming an observed color excess to the amount of extinction following a certain extinction law. It is customary to assume that the reddening is linear and not dependent on the type of the object, and the transformation is usually carried out with an assumption that a single, linear reddening vector for a given filter set can be applied to various objects with different SEDs. To quantify the error involved in the extinction estimation using these two assumptions, we define a “reference extinction law” as the amount of extinction relative to 5500 Å ( $A_i/A_{5500}$ ) that an imaginary filter having a Dirac delta transmission function at  $\lambda_c$  of an SDSS filter  $i$  would experience for the SED of a 10 Gyr elliptical galaxy at redshift  $z$  of 0 when  $A_{5500} = 0.1$ . Table 2 gives  $A_i/A_{5500}$  values for the SDSS filters and the reddening vectors calculated from this extinction law will be called “reference reddening vectors.”

The amount of extinction estimated from a calculated color excess and the reference reddening vector will be labeled by  $A^{est}$  (this is our “simulated” amount of extinction that one would estimate from observed color excess in practice when not considering the SED-dependence and nonlinearity of the reddening). In our analyses below, we will describe the behaviors of reddening in terms of the values ( $A^{est} - A^{act}$ ).

Figure 2 shows the SED dependence and nonlinearity

of the extinction in two sample CM diagrams of nine different pairs of SDSS filters. The discrepancies between the actual (symbol) and reference (line) reddenings are generally larger 1) for the filter pairs involving the  $g$  filter, and 2) for the elliptical galaxy. The former is because the  $g$  filter has a much larger  $\Delta\lambda/\lambda_c$  ratio than the other filters (see Table 1), and this causes the central wavelength of  $g$  to shift more significantly than the others as the extinction becomes larger. The fact that the reddening becomes noticeably nonlinear when one of the two filters has a large  $\Delta\lambda/\lambda_c$  was also observed in the near-infrared CM diagrams (see Kim et al. 2005, 2006).

The reason that the elliptical galaxy shows larger discrepancies is a bit more complex. In the wavelength regime of the  $g$  filter, the elliptical galaxy has nearly flat or increasing  $f_\lambda$  with increasing  $\lambda$  while the irregular galaxy has decreasing  $f_\lambda$  (see Fig. 1). Thus, in the limit of small extinction, the effective wavelengths,

$$\lambda_{eff} = \exp \frac{\int d(\ln \nu) f_\nu S_\nu \ln \lambda}{\int d(\ln \nu) f_\nu S_\nu}, \quad (5)$$

of the elliptical galaxy are longer than  $\lambda_c$ , and, for example, the  $u - g$  ( $g - r$ ) reddening curve of the elliptical galaxy is shallower (steeper) than the reference reddening vector. Conversely, for the irregular galaxy, the  $u - g$  ( $g - r$ ) reddening curve is steeper (shallower) than the reference reddening vector. As the extinction becomes more significant,  $\lambda_{eff}$  values shift to longer wavelengths, and the reddening curves for  $u - g$  ( $g - r$ ) become shallower (steeper) for both elliptical and irregular galaxies. Therefore, as the extinction increases, the discrepancies between the actual and reference reddenings for both  $u - g$  and  $g - r$  colors become larger for the elliptical galaxy but smaller for the irregular galaxy.

Figure 3 shows the SED-dependence and nonlinearity of the extinction in CC diagrams for four different color combinations of SDSS filters. As in Figure 2, the discrepancies between the actual and reference reddenings are more significant for the color combinations involving the  $g$  filter and for the elliptical galaxy. The behavior of the actual reddening curve relative to the reference reddening vector can be explained similarly to that in the CM diagrams. As an example, here we describe the reddening behavior in the  $u - g$  vs.  $g - r$  diagram in detail. In the limit of small extinction for the elliptical galaxy, the

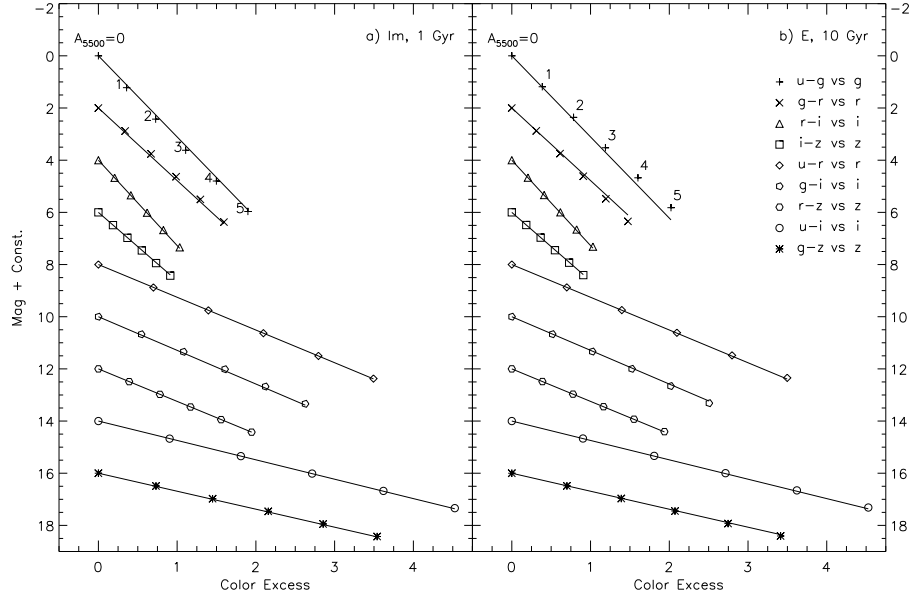


FIG. 2.— The symbols show the actual reddening curves of 1 Gyr (a) and 10 Gyr (b) galaxies at redshift  $z = 0$  for nine different color-magnitude diagrams of SDSS filters. The distance between adjacent symbols in each curve corresponds to the extinction of one magnitude at 5500 Å ( $A_{5500} = 1$ ). The lines show the “reference” reddening vectors of the corresponding filter set, whose slope is obtained with the reference extinction law in Table 2. The largest deviations from the linear relation are for the  $u-g$  and  $g-r$  colors, and are in a different sense for 1 Gyr vs. 10 Gyr galaxy SEDs. The largest deviations from the reference reddening vector are also for the  $u-g$  and  $g-r$  colors and for the elliptical galaxy.

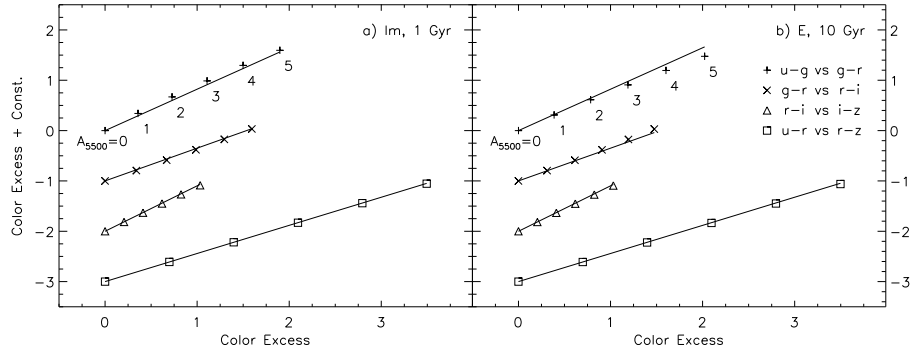


FIG. 3.— Same as Figure 2, but for four different color-color diagrams.

actual  $u-g$  ( $g-r$ ) color excess is larger (smaller) than the reference color excess (because  $\lambda_{eff} - \lambda_c$  is larger for  $g$ ), and this makes the actual reddening curve in  $u-g$  vs.  $g-r$  CC diagram shallower than the reference reddening vector. As the extinction becomes larger, the  $\lambda_{eff}$  of  $g$  increases more rapidly than that of  $u$  and  $r$ , and the  $u-g$  ( $g-r$ ) color excess becomes larger (smaller) more quickly compared to the reference color excess. This makes the actual reddening curve in the  $u-g$  vs.  $g-r$  diagram deviate further from the reference vector as the extinction increases.

We now discuss the way the SED dependence and non-linearity of the extinction cause errors in estimating the amount of extinction from the observed colors. Figures 4–5 show the differences between  $A^{est}$  and  $A^{act}$  in nine colors for our 1, 3, and 10 Gyr galaxy models.  $A^{est}$  is the amount of extinction estimated from the calculated

color excess and our reference extinction law in Table 2. That is,  $A^{est}$  is estimated by

$$A_Y^{est} = \frac{(m_X - m_Y) - (m_X - m_Y)_0}{A_X^{ref}/A_Y^{ref} - 1}, \quad (6)$$

where  $m_X$  and  $m_Y$  are the reddened magnitudes of two filters,  $X$  and  $Y$ , the subscript 0 denotes the intrinsic value, and  $A_X^{ref}/A_Y^{ref}$  is our reference extinction law between the two filters. The figures show that in general, the discrepancies between  $A^{est}$  and  $A^{act}$  are larger for older isochrones and colors involving the  $g$  filter, as expected from Figure 2. This implies, for example, that applying to late-type galaxies a reddening curve calculated for an early-type galaxy may cause a non-negligible error in dereddening, particularly for colors involving  $g$ . Moreover, although the overall  $A^{est} - A^{act}$  values are

relatively small for colors involving the  $g$  filter at 1 Gyr, their reddening curves are nonlinear at all ages. The largest relative difference of  $|A^{est} - A^{act}|$  between different 10 Gyr galaxies is 9 % and occurs in  $u - g$  between the elliptical and irregular galaxies at  $A_g^{est} \sim 1$ .

It is worth noting that the colors between  $r$ ,  $i$  and  $z$  show very little SED dependence and nonlinearity. This is because these filters are located near the Rayleigh-Jeans regime of the stellar spectra, and thus the colors between them are almost identical for all SEDs.

The colors involving two filters whose  $\lambda_c$ 's are further apart exhibit smaller SED dependence and nonlinearity (e.g.,  $u - i$  has smaller SED dependence and nonlinearity of extinction than  $u - g$  and  $u - r$ ). This is because the shift of  $\lambda_{eff}$  due to extinction becomes relatively less significant as the gap between the two  $\lambda_{eff}$  (or  $\lambda_c$ ) values increases.

Figure 6 shows the  $A^{est} - A^{act}$  values for three different redshift values ( $z = 0, 0.1$ , and  $0.2$ ) of four galaxy morphologies at 3 Gyr. The dependence of reddening curves on  $z$  is not negligible for  $z$  values between 0 and 0.2. Again, the colors involving the  $g$  filter show the largest variations of  $A^{est} - A^{act}$  between different  $z$  values. This is because the dependence of the SED slope on  $z$  is the largest in the  $g$  filter, which is due to the Balmer break (see Fig. 7). As  $z$  increases, the SED slope in the  $g$  filter increases to a more positive value and  $\lambda_{eff}$  shifts to a longer wavelength. Thus in case of  $u - g$  vs.  $g - r$  vs.  $r$  CM diagram, the reddening vector becomes shallower (steeper) and  $A^{est} - A^{act}$  becomes larger (smaller).

The procedure for calculating the correct amount of extinction from an observed color excess is then 1) to obtain  $A^{est}$  from an observed color excess and our reference extinction law in Table 2, and 2) to correct it with the corresponding  $A^{est} - A^{act}$  value in Figures 4 to 6, i.e. to subtract  $A^{est} - A^{act}$  from  $A^{est}$ .<sup>5</sup> As our  $A^{est}$  and  $A^{act}$  values are calculated with the redshifted spectra, any  $K$ -corrections can be applied independently from our dereddening procedures.

Figures 4 through 6 cannot effectively show the SED-dependence of the reddening at low extinction. This can be manifested with  $A^{est}/A^{act}$ , instead of  $A^{est} - A^{act}$ . Figure 8 clearly shows that the SED-dependence of the reddening is present even at low extinction and that the  $A^{est}/A^{act}$  ratio is a very weak function of extinction.

Schlegel et al. (1998) gives the relative extinctions for the SDSS filters that are calculated for a  $z = 0$  elliptical galaxy SED using the SDSS filter response functions published by Fukugita et al. (1996). These response functions are somewhat different from the most recent ones available, which are the ones adopted in the present work, and result in relative extinction values that are different from our reference extinction law by upto  $\sim 7$  % (Table 2; the difference is largest in  $z$  while smaller than 3 % in  $u$  and  $g$ ). Figure 9 shows the  $A^{est} - A^{act}$  values where  $A^{est}$  are calculated with the relative extinctions by Schlegel et al. instead of our reference extinction law. Most of the  $A^{est} - A^{act}$  values are negative, meaning that using the relative extinctions by Schlegel et al. would underestimate the amount of extinction in most cases by  $\sim 5$  to 10 % (maximum  $\sim 20$  %). This is because the

relative extinctions by Schlegel et al. have a stronger wavelength dependence compared to our values (see eq. 6).

### 3.2. Extinction Values in the SDSS Archive

The SDSS archive provides the amount of Galactic extinction in  $r$  magnitude at the position of each object that is computed following the relative extinction by Schlegel et al. (1998; Table 2). For the reasons discussed above, the relative extinction depends on the SED of an object and on the amount of extinction, which is not considered in the extinction values given in the SDSS archive. In Tables 3 to 5, we provide the coefficients of the best-fit polynomials to  $A_i$  as a function of  $A_{5500}$  for our 3 and 10 Gyr galaxy models (valid for  $A_{5500} \leq 5$  mag). The fitting polynomial has a form of

$$A_i = c_1 A_{5500} + c_2 (A_{5500})^2 + c_3 (A_{5500})^3. \quad (7)$$

In order to correct the extinction value given in the SDSS archive, one first divides the  $r$  extinction value of the archive by 0.843 to obtain  $A_{5500}$  (that is,  $A_V$ ), and use equation (7) to obtain  $A_i$ . Here, 0.843 is the  $A_r/A_V$  value calculated by Schlegel et al. (1998) using the SDSS filter response functions by Fukugita et al. (1996). We find that the largest correction in  $r$  for  $A_{5500} = 2.5$  mag made by this procedure is 0.09 mag, and most of the correction comes from the new filter response functions that we use. The SED-dependence and nonlinearity of the extinction results in corrections in  $r$  of less than 0.035 mag at  $A_{5500} = 2.5$  mag, which is much less than the corrections for the dereddening from the color excesses discussed above. This shows that small differences in the relative extinction (i.e., extinction law) result in relatively large differences in the estimated extinction from the color excess.

### 3.3. Estimation of Morphology and Redshift from CC Diagrams

As the reddening behavior is dependent on the morphology and redshift of the galaxy, one needs to know this information before applying our fitting formulae. When visual inspection is not practical or feasible, one could use the Petrosian inverse concentration index (Strateva et al. 2001, Shimasaku et al. 2001), Sérsic index (Blanton et al. 2003), Gini coefficient (Abraham, van den Bergh, & Nair 2003), coarseness parameter (Yamauchi et al. 2005), or radial color gradient (Park & Choi 2005) as a measure of the morphology of galaxies. Alternatively, one could estimate the morphology from the location in the CC diagram. Figure 10 shows the intrinsic colors of our model galaxies along with the reddening curves. There are cases where one galaxy is located near the reddening curve of another galaxy of different morphology. In such cases, one would need an approximate value of extinction based on the spatial location of the galaxy in the sky from, e.g., Schlegel et al. (1998) to disentangle the degeneracy.

When the redshift of the galaxy is not known (e.g., when the spectrum is not available), it needs to be estimated from the colors as well. Figure 10 shows that the directions of the increasing reddening and redshift are separated the most in  $u - g$  vs.  $g - r$  CC diagram for small  $z$  values ( $\lesssim 0.2$ ), primarily due to the Balmer break. But in most cases, the redshift is degenerate with

<sup>5</sup> An electronic table of  $A^{est} - A^{act}$  values is available from the authors upon request.

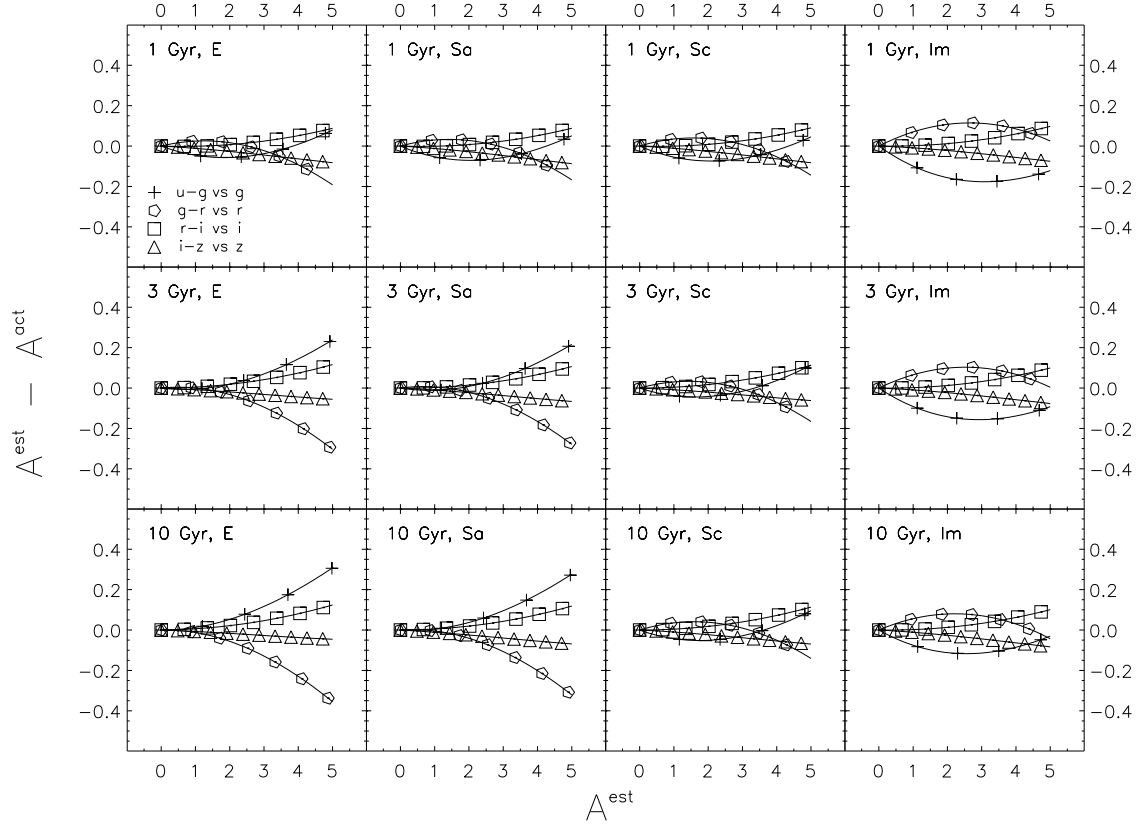


FIG. 4.— The differences between the estimated extinction  $A^{est}$  and the actual extinction  $A^{act}$  in four different color-magnitude diagrams for our  $z = 0$  galaxy models (four morphologies and three ages). See the text for the definitions of  $A^{est}$  and  $A^{act}$ . The distance between adjacent symbols in each curve corresponds to the extinction of one magnitude at  $5500 \text{ \AA}$ .

TABLE 3  
COEFFICIENTS OF BEST-FIT POLYNOMIALS TO  $A_i$  AS A FUNCTION OF  $A_{5500}$  FOR  $z=0$  GALAXIES<sup>a</sup>

Morphology	Filter	3 Gyr			10 Gyr		
		$c_1$	$c_2$	$c_3$	$c_1$	$c_2$	$c_3$
E	<i>u</i>	1.574	-1.25E-03	1.33E-05	1.574	-1.20E-03	1.17E-05
E	<i>g</i>	1.197	-6.52E-03	1.46E-04	1.192	-6.25E-03	1.41E-04
E	<i>r</i>	0.877	-1.44E-03	6.25E-06	0.876	-1.44E-03	7.21E-06
E	<i>i</i>	0.672	-1.57E-03	1.40E-06	0.671	-1.56E-03	1.35E-06
E	<i>z</i>	0.487	-1.03E-03	-3.36E-06	0.487	-1.04E-03	-3.19E-06
Sa	<i>u</i>	1.574	-1.27E-03	1.36E-05	1.575	-1.23E-03	1.32E-05
Sa	<i>g</i>	1.199	-6.63E-03	1.48E-04	1.195	-6.40E-03	1.44E-04
Sa	<i>r</i>	0.877	-1.44E-03	6.61E-06	0.876	-1.44E-03	7.23E-06
Sa	<i>i</i>	0.672	-1.56E-03	6.60E-07	0.671	-1.57E-03	2.02E-06
Sa	<i>z</i>	0.488	-1.03E-03	-3.14E-06	0.487	-1.03E-03	-3.03E-06
Sc	<i>u</i>	1.577	-1.38E-03	1.57E-05	1.578	-1.39E-03	1.53E-05
Sc	<i>g</i>	1.209	-7.07E-03	1.51E-04	1.211	-7.14E-03	1.50E-04
Sc	<i>r</i>	0.878	-1.45E-03	6.87E-06	0.878	-1.45E-03	6.94E-06
Sc	<i>i</i>	0.673	-1.57E-03	1.87E-06	0.673	-1.57E-03	1.05E-06
Sc	<i>z</i>	0.488	-1.03E-03	-2.48E-06	0.488	-1.02E-03	-2.84E-06
Im	<i>u</i>	1.579	-1.45E-03	1.52E-05	1.579	-1.44E-03	1.61E-05
Im	<i>g</i>	1.226	-7.62E-03	1.44E-04	1.221	-7.48E-03	1.47E-04
Im	<i>r</i>	0.881	-1.47E-03	5.77E-06	0.880	-1.46E-03	6.15E-06
Im	<i>i</i>	0.675	-1.56E-03	-1.06E-06	0.674	-1.56E-03	-4.35E-08
Im	<i>z</i>	0.490	-9.92E-04	-4.02E-06	0.490	-9.97E-04	-3.87E-06

<sup>a</sup> The coefficients are to be used with the fitting formula of equation (7), which is valid for  $A_{5500} \leq 5 \text{ mag}$ .

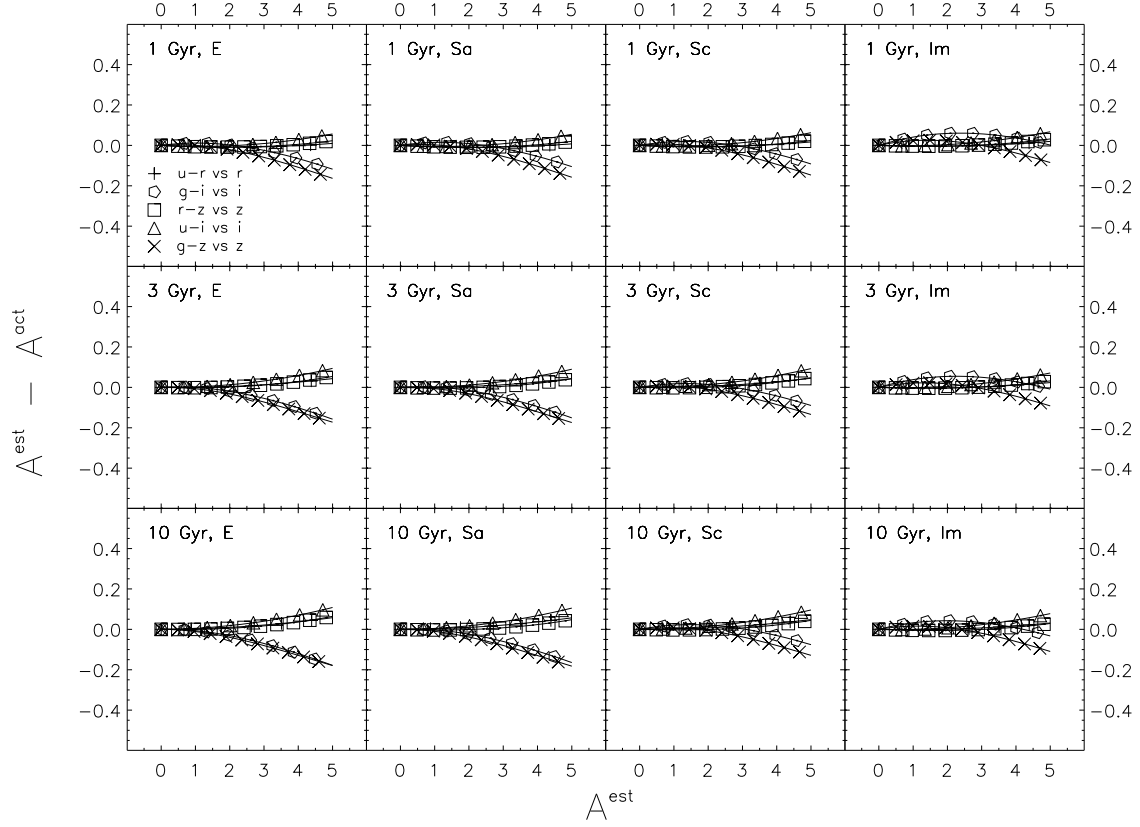


FIG. 5.— Same as Figure 4, but for five more color-magnitude diagrams.

 TABLE 4  
 COEFFICIENTS OF BEST-FIT POLYNOMIALS TO  $A_i$  AS A FUNCTION OF  $A_{5500}$  FOR  $z=0.1$  GALAXIES<sup>a</sup>

Morphology	Filter	3 Gyr			10 Gyr		
		$c_1$	$c_2$	$c_3$	$c_1$	$c_2$	$c_3$
E	<i>u</i>	1.572	-1.16E-03	1.22E-05	1.569	-1.09E-03	1.13E-05
E	<i>g</i>	1.178	-5.88E-03	1.49E-04	1.172	-5.65E-03	1.51E-04
E	<i>r</i>	0.874	-1.42E-03	8.13E-06	0.873	-1.41E-03	8.58E-06
E	<i>i</i>	0.672	-1.59E-03	7.55E-07	0.671	-1.60E-03	1.29E-06
E	<i>z</i>	0.488	-1.02E-03	-2.81E-06	0.488	-1.02E-03	-3.23E-06
Sa	<i>u</i>	1.573	-1.19E-03	1.29E-05	1.571	-1.15E-03	1.17E-05
Sa	<i>g</i>	1.181	-6.02E-03	1.52E-04	1.176	-5.85E-03	1.53E-04
Sa	<i>r</i>	0.875	-1.43E-03	8.71E-06	0.874	-1.41E-03	8.33E-06
Sa	<i>i</i>	0.672	-1.59E-03	1.35E-06	0.671	-1.60E-03	1.68E-06
Sa	<i>z</i>	0.488	-1.01E-03	-3.78E-06	0.488	-1.01E-03	-3.66E-06
Sc	<i>u</i>	1.580	-1.33E-03	1.40E-05	1.581	-1.35E-03	1.38E-05
Sc	<i>g</i>	1.194	-6.45E-03	1.50E-04	1.197	-6.54E-03	1.49E-04
Sc	<i>r</i>	0.876	-1.43E-03	7.11E-06	0.876	-1.44E-03	7.32E-06
Sc	<i>i</i>	0.673	-1.58E-03	4.58E-07	0.673	-1.58E-03	-1.08E-07
Sc	<i>z</i>	0.489	-1.01E-03	-3.26E-06	0.489	-1.00E-03	-4.42E-06
Im	<i>u</i>	1.584	-1.41E-03	1.52E-05	1.583	-1.40E-03	1.56E-05
Im	<i>g</i>	1.211	-6.85E-03	1.36E-04	1.207	-6.76E-03	1.41E-04
Im	<i>r</i>	0.880	-1.47E-03	6.83E-06	0.879	-1.46E-03	7.61E-06
Im	<i>i</i>	0.675	-1.58E-03	-1.49E-07	0.675	-1.58E-03	3.68E-07
Im	<i>z</i>	0.490	-9.98E-04	-3.60E-06	0.490	-1.00E-03	-3.31E-06

<sup>a</sup> The coefficients are to be used with the fitting formula of equation (7), which is valid for  $A_{5500} \leq 5$  mag.

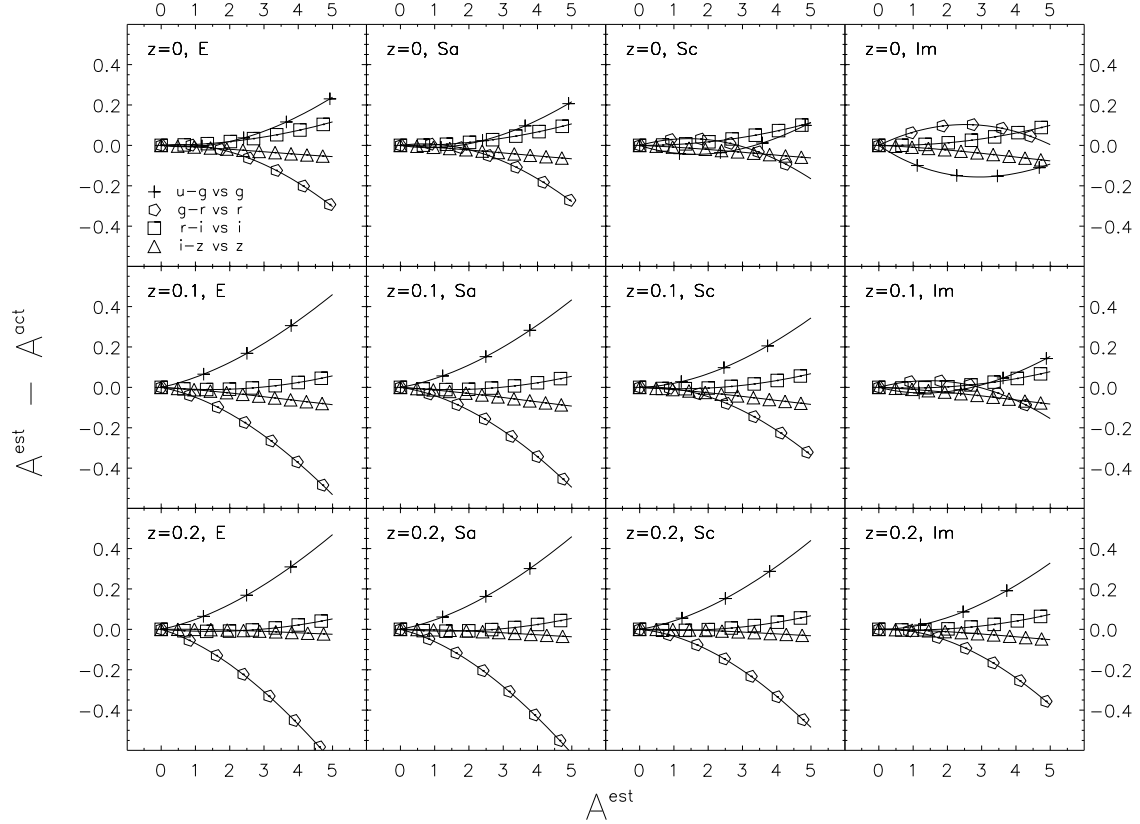


FIG. 6.— Same as Figure 4, but for our 3 Gyr galaxy models with redshift values of 0, 0.1, and 0.2 in four different SDSS colors.

TABLE 5  
COEFFICIENTS OF BEST-FIT POLYNOMIALS TO  $A_i$  AS A FUNCTION OF  $A_{5500}$  FOR  $z=0.2$  GALAXIES<sup>a</sup>

Morphology	Filter	3 Gyr			10 Gyr		
		$c_1$	$c_2$	$c_3$	$c_1$	$c_2$	$c_3$
E	<i>u</i>	1.565	-1.06E-03	1.28E-05	1.562	-1.04E-03	1.27E-05
E	<i>g</i>	1.174	-6.17E-03	1.75E-04	1.170	-6.19E-03	1.80E-04
E	<i>r</i>	0.875	-1.46E-03	7.98E-06	0.873	-1.46E-03	9.01E-06
E	<i>i</i>	0.672	-1.57E-03	4.38E-07	0.671	-1.58E-03	1.48E-06
E	<i>z</i>	0.487	-1.01E-03	-3.28E-06	0.486	-1.02E-03	-2.27E-06
Sa	<i>u</i>	1.568	-1.13E-03	1.41E-05	1.567	-1.13E-03	1.39E-05
Sa	<i>g</i>	1.177	-6.28E-03	1.75E-04	1.174	-6.32E-03	1.80E-04
Sa	<i>r</i>	0.875	-1.46E-03	8.09E-06	0.874	-1.47E-03	9.69E-06
Sa	<i>i</i>	0.672	-1.57E-03	8.19E-07	0.672	-1.57E-03	5.86E-07
Sa	<i>z</i>	0.487	-1.01E-03	-3.18E-06	0.486	-1.01E-03	-2.68E-06
Sc	<i>u</i>	1.579	-1.35E-03	1.50E-05	1.581	-1.37E-03	1.47E-05
Sc	<i>g</i>	1.187	-6.55E-03	1.73E-04	1.190	-6.66E-03	1.74E-04
Sc	<i>r</i>	0.877	-1.47E-03	7.63E-06	0.877	-1.48E-03	7.42E-06
Sc	<i>i</i>	0.673	-1.58E-03	5.63E-07	0.673	-1.57E-03	3.32E-07
Sc	<i>z</i>	0.488	-1.00E-03	-3.81E-06	0.488	-1.01E-03	-3.19E-06
Im	<i>u</i>	1.584	-1.41E-03	1.56E-05	1.583	-1.39E-03	1.46E-05
Im	<i>g</i>	1.199	-6.82E-03	1.68E-04	1.196	-6.75E-03	1.70E-04
Im	<i>r</i>	0.881	-1.48E-03	5.95E-06	0.880	-1.48E-03	6.59E-06
Im	<i>i</i>	0.676	-1.57E-03	-4.14E-07	0.675	-1.57E-03	-3.46E-07
Im	<i>z</i>	0.490	-9.94E-04	-3.53E-06	0.489	-9.95E-04	-3.91E-06

<sup>a</sup> The coefficients are to be used with the fitting formula of equation (7), which is valid for  $A_{5500} \leq 5$  mag.



TABLE 6  
INTRINSIC COLORS OF OUR GALAXY MODELS<sup>a</sup>

Redshift	Morphology	3 Gyr				10 Gyr			
		$u-g$	$g-r$	$r-i$	$i-z$	$u-g$	$g-r$	$r-i$	$i-z$
0.0	E	1.51	0.69	0.32	0.24	1.66	0.80	0.38	0.28
0.0	Sa	1.41	0.65	0.29	0.21	1.53	0.74	0.36	0.25
0.0	Sc	1.07	0.48	0.24	0.19	1.00	0.45	0.24	0.18
0.0	Im	0.64	0.11	0.07	0.06	0.76	0.23	0.13	0.09
0.1	E	1.56	0.87	0.35	0.28	1.70	1.00	0.41	0.34
0.1	Sa	1.46	0.82	0.33	0.26	1.56	0.93	0.39	0.31
0.1	Sc	1.05	0.59	0.26	0.22	0.97	0.55	0.25	0.22
0.1	Im	0.64	0.18	0.06	0.07	0.75	0.30	0.13	0.12
0.2	E	1.61	1.14	0.43	0.29	1.80	1.30	0.49	0.34
0.2	Sa	1.48	1.07	0.40	0.27	1.59	1.20	0.46	0.32
0.2	Sc	0.89	0.78	0.31	0.22	0.80	0.72	0.29	0.22
0.2	Im	0.48	0.33	0.08	0.06	0.59	0.46	0.15	0.12

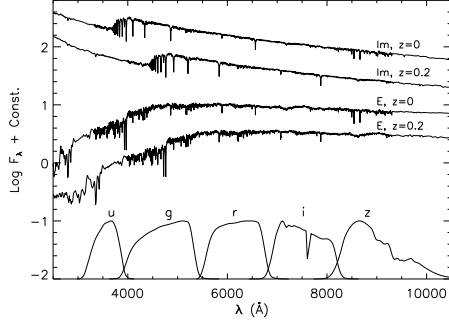


FIG. 7.— Spectra of elliptical and irregular galaxies at 3 Gyr for two redshift values  $z = 0$  and  $0.2$ . Also shown are the response functions of the SDSS filters for 1.3 airmasses.

the reddening, and the SED-dependence and nonlinearity of the reddening need to be incorporated into the estimation of the redshift from photometric data.

Figure 11 shows that our synthetic galaxy colors roughly agree with the visually classified catalog of SDSS galaxies by Fukugita et al. (2007) nearly within the dispersion of each morphology class. Late-type galaxies show larger discrepancies, probably because the population synthesis model of Buzzoni (2005) does not include the effect of internal dust, which suppresses ultraviolet emission. This effect would result in bluer colors in short-wavelength filters ( $u - g$  &  $g - r$ ) for late-type galaxies (Sc and Im), and this fact needs to be taken into account when our fitting formulae are applied to visually classified galaxies.

#### 4. SUMMARY

We have analyzed the behaviors of reddening curves in color-magnitude and color-color diagrams of the SDSS photometric system for various galaxy models with redshift values up to  $0.2$ .

We have shown that the SED-dependence and the nonlinearity of the reddening in the SDSS filters are not negligible. These behaviors are the most significant for colors involving the  $g$  filter, which has the largest  $\Delta\lambda/\lambda_c$  value among SDSS filters.

The SDSS colors involving adjacent filters have greater SED-dependence and nonlinearity because the shift of  $\lambda_{eff}$  due to extinction becomes relatively more significant as the gap between the two  $\lambda_{eff}$  (or  $\lambda_c$ ) values decreases.

To provide a procedure to calculate the correct amount of extinction from an observed color excess, we defined a “reference extinction law” that an imaginary filter having a Dirac delta transmission function at  $\lambda_c$  of an SDSS filter  $i$  would experience for the SED of a 10 Gyr elliptical galaxy when  $A_{5500} = 0.1$ . In order to calculate the amount of extinction for a given object, one first obtains  $A^{est}$  from an observed color excess and our reference reddening vector, then corrects it with the corresponding  $A^{est} - A^{act}$  value in Figures 4 to 6.

The relative extinctions between (i.e., the extinction law for) SDSS filters given by Schlegel et al., which were calculated with an older version of filter response functions, would underestimate the amount of extinction in most cases by  $\sim 5$  to  $10\%$  (maximum  $\sim 20\%$ ). Our reference extinction law in Table 2 is recommended instead when the extinction is small (i.e., when the nonlinearity and SED-dependence are not important, or  $A < 1$ ).

Finally, we have shown that the dependence of reddening on redshift at low extinction is the largest for colors involving the  $g$  filter as well, which is due to the Balmer break.

We thank Yun-Young Choi, Myungshin Im, Juhan Kim, Sang Chul Kim, Hwankyung Sung, and Suk-Jin Yoon for helpful discussion. We also deeply thank the anonymous referee, whose comments greatly improved our manuscript. S. S. K. was supported by the Astrophysical Research Center for the Structure and Evolution of the Cosmos (ARCSEC) of the Korea Science and Engineering Foundation through the Science Research Center (SRC) program. M. G. L. was in part supported by ABRL (R14-2002-058-01000-0). This work was in part supported by the BK21 program as well.

#### REFERENCES

- Abraham, R. G., van den Bergh, S., & Nair, P. 2003, *ApJ*, 588, 218  
 Blanton, M. R. et al. 2003, *ApJ*, 594, 186  
 Bruzual, G., & Charlot, S. 2003, *MNRAS*, 344, 1000  
 Buzzoni, A. 2005, *MNRAS*, 361, 725  
 Cardelli, J. A., Clayton, G. C., & Mathis, J. S. 1989 *ApJ*, 345, 245  
 Chabrier, G. 2003, *PASP*, 115, 763  
 Fiorucci, M., & Munari, U. 2003, *A&A*, 401, 781  
 Fukugita, M., Ichikawa, T., Gunn, J. E., Doi M., Shimasaku, K., & Schneider, D. P. 1996, *AJ*, 111, 1748  
 Fukugita, M. et al. 2007, *AJ*, 134, 579  
 Girardi, L., Grebel, E. K., Odenkirchen, M., & Chiosi, C. 2004, *A&A*, 422, 205 (GGOC)  
 Grebel, E. K., & Roberts, W. J. 1995, *A&AS*, 109, 293  
 Kim, S. S., Figer, D. F., Lee, M. G., & Oh, S. 2005, *PASP*, 117, 445  
 Kim, S. S., Figer, D. F., & Lee, M. G. 2006, *PASP*, 118, 62  
 Oke, J. B., & Gunn, J. E. 1983, *ApJ*, 266, 713  
 Park, C., & Choi, Y.-Y. 2005, 635, L29  
 Schlegel, D. J., Finkbeiner, D. P., & Davis, M. 1998, *ApJ*, 500, 525  
 Schneider, D. P., Gunn, J. E., & Hoessel, J. G. 1983, *ApJ*, 264, 337  
 Shimasaku, K. et al. 2001, *AJ*, 122, 1238  
 Stoughton, C., Lupton, R. H., Bernardi, M., Blanton, M. R., Burles, S., Castander, F. J., Connolly, A. J. et al. 2002, *AJ*, 123, 485  
 Strateva, I. et al. 2001, *AJ*, 122, 1861  
 Yamauchi, C. et al. 2005, *AJ*, 130, 1545

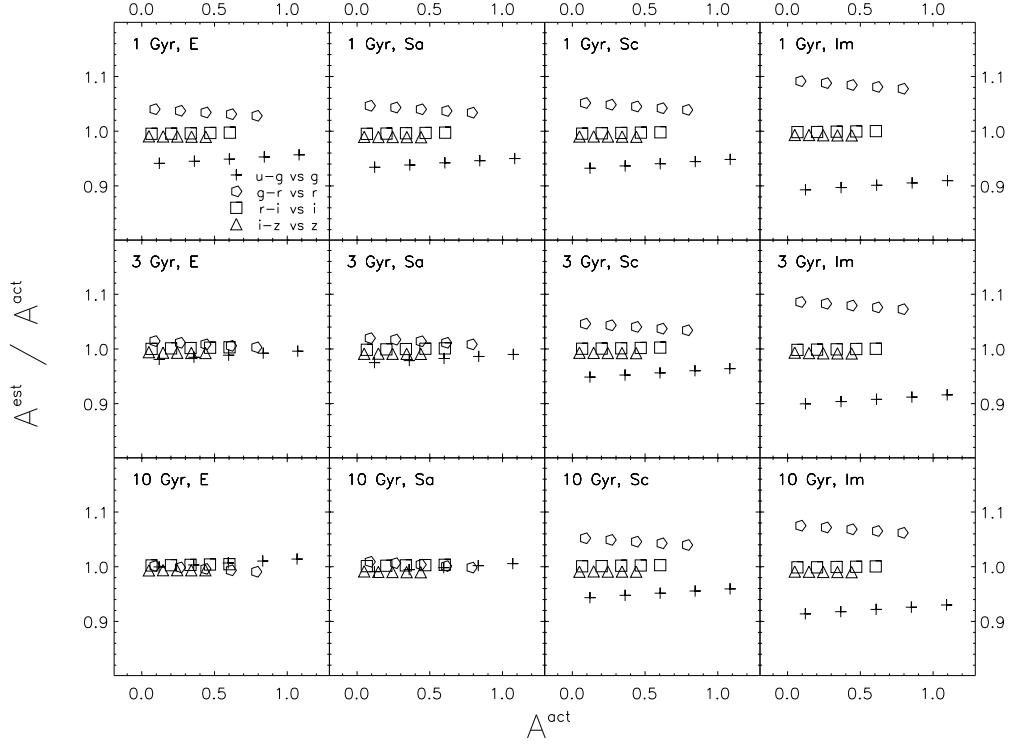


FIG. 8.— The ratios between the estimated extinction  $A^{est}$  and the actual extinction  $A^{act}$  in four different color-magnitude diagrams for our  $z = 0$  galaxy models (four morphologies and three ages). See the text for the definitions of  $A^{est}$  and  $A^{act}$ . This plot is to show the SED-dependence of reddening at low extinction. Each symbol, from left to right, represents extinction values of 0.1, 0.3, 0.5, 0.7, and 0.9 mag at 5500 Å.

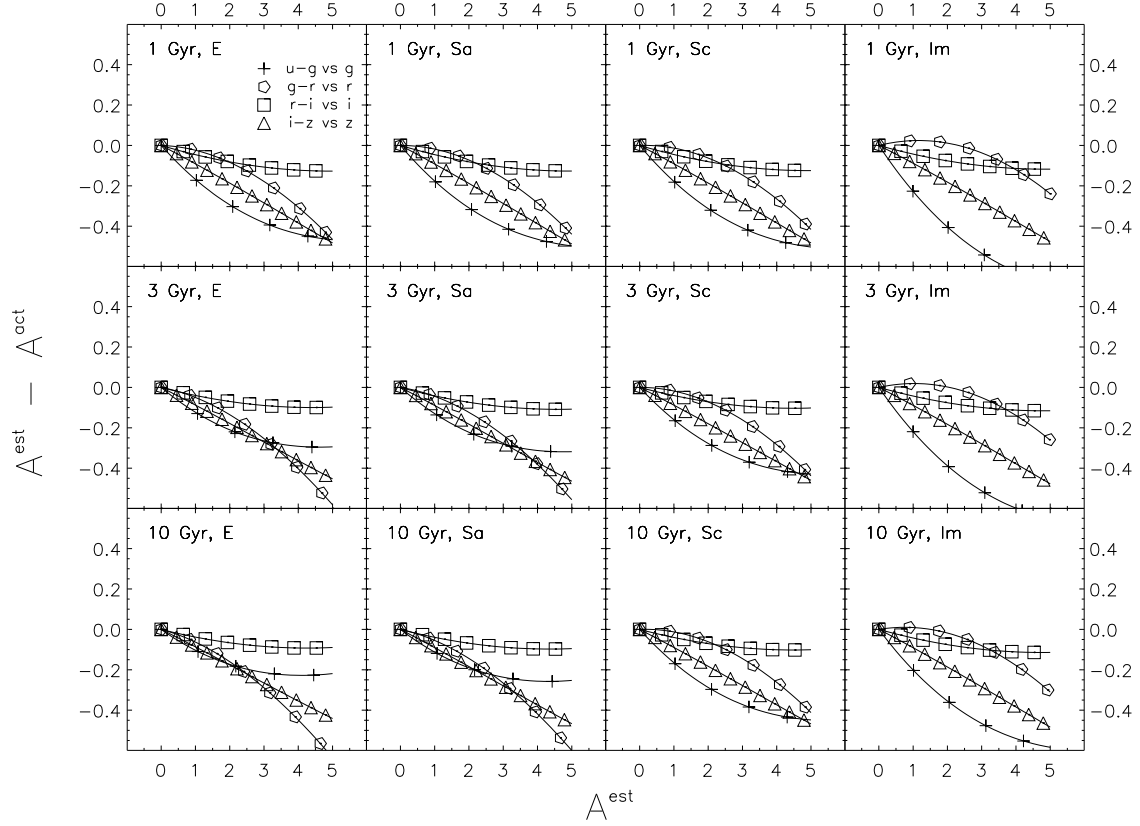


FIG. 9.— Same as Figure 4, but  $A^{est}$  values are calculated with the relative extinctions by Schlegel et al. (1998) instead of our reference extinction law.

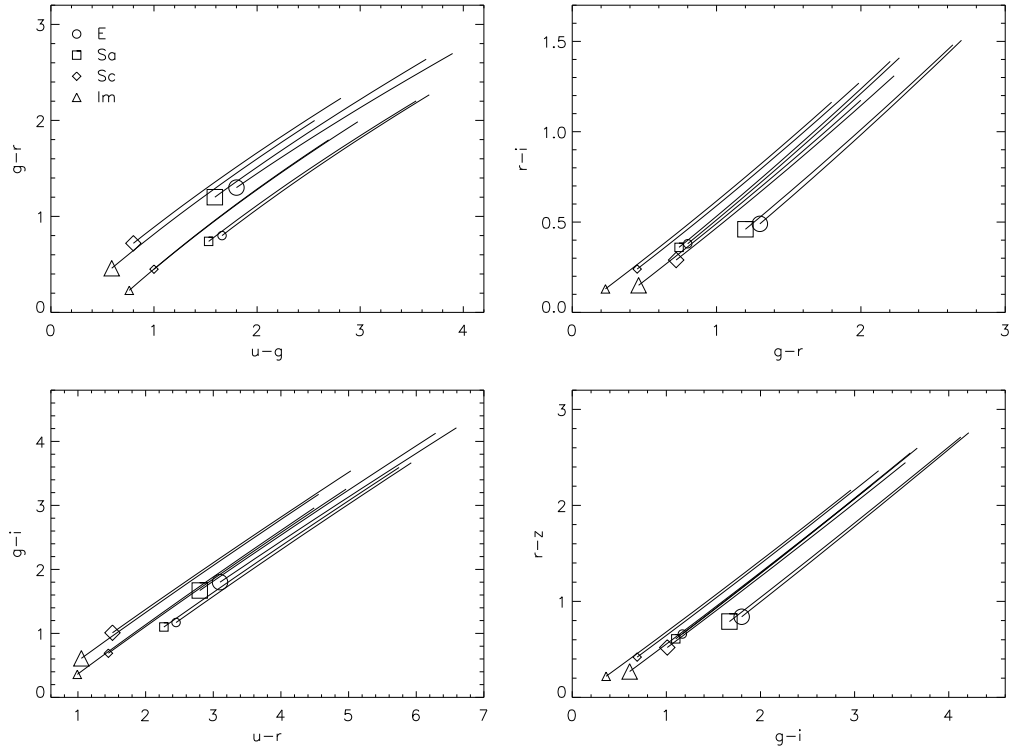


FIG. 10.— Intrinsic colors of our 10 Gyr galaxy models (symbols) in four color-color diagrams along with their reddening curves (lines). Small symbols are for  $z = 0$  models and large symbols for  $z = 0.2$ . The length of the reddening curve corresponds to  $A_{5500} = 5$  mag.

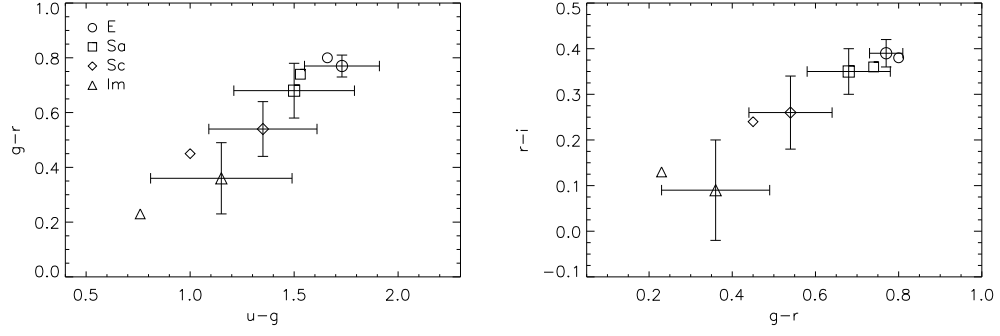


FIG. 11.— Intrinsic colors of our 10 Gyr,  $z = 0$  galaxy models (symbols) and the mean colors of visually classified SDSS galaxies after  $K$ -correction by Fukugita et al. (2007; symbols with error bars). Error bars represent the dispersion.